Materials Advances

ROYAL SOCIETY OF CHEMISTRY

PAPER

View Article Online
View Journal | View Issue

Cite this: *Mater. Adv.*, 2025, 6, 6479

Planar *vs.* twisted pyrimidine derivatives: insights from molecular dynamics and predictive modelling for melamine detection in dairy products†

Harshal V Barkale,[a] Bappa Maiti[b] and Nilanjan Dey *[a]

Herein, we report the design and synthesis of two pyrimidine derivatives with different donor substituents, pyrene (**1**) and anthracene (**2**), that show aggregation in an aqueous medium. The aggregates of compound **1** were found to be pH-sensitive as well as thermoresponsive. The energy-optimized structure of compound **1** revealed a nearly planar conformation with a dihedral angle of ~0.2° between the donor and the acceptor moieties, which appeared to be ~50.8° for compound **2**. A 2.5-fold and 5-fold turn-on fluorescence response was observed after the addition of melamine for compounds **1** and **2**, respectively. Importantly, compound **1** was successfully applied for the quantification of melamine in real milk products, with high recovery rates, and the results were validated using liquid chromatography-mass spectrometry (LC-MS). Accurate estimation of melamine levels was achieved with a limit of detection (LOD) of 0.8 ppm, well below regulatory thresholds. Furthermore, we developed chemically modified paper strips capable of detecting melamine directly in adulterated milk samples without any instrumentation, offering a practical and low-cost on-site screening method. To gain mechanistic insight, molecular dynamics (MD) simulations were employed to analyze the stability, interaction energies, and aggregation tendencies of the compounds. The self-assembled structures of **1** after 120 ns showed an anti-parallel arrangement with the pyrene moiety of one molecule π-stacked with the pyrimidine unit of another molecule. In contrast, compound **2** exhibited face-to-face π-stacking among anthracene moieties and multiple hydrogen bonds (1.8–2.2 Å) among pyrimidine residues. Finally, various machine learning models were used to predict melamine intensity from concentration *vs.* fluorescence data. The linear regression model (R^2 = 0.9959) delivered the best performance, reinforcing the efficiency of linear approaches in this dataset.

Received 11th May 2025,
Accepted 18th July 2025

DOI: 10.1039/d5ma00470e

rsc.li/materials-advances

Introduction

Complementary hydrogen bonding is a fundamental interaction in nature, playing a critical role in the structure and function of many biological and chemical systems. From the double-helix structure of DNA, stabilized by complementary hydrogen bonds between base pairs, to the folding and stability of proteins, hydrogen bonding enables precise molecular recognition and interaction.[1] In addition to biological processes, hydrogen bonding is also critical for recognizing neutral biomolecules such as melamine, which has significant industrial and health implications. Melamine (1,3,5-triazine-2,4,6-triamine), with three exocyclic amine groups, exhibits unique supramolecular recognition features due to its ability to act as both a hydrogen bond donor and acceptor, forming extended networks through complementary interactions. This makes melamine an ideal scaffold for constructing hydrogen-bonded assemblies in both crystal engineering and solution-based sensing platforms. Melamine has 67% nitrogen by mass, and has been illegally added to food (*e.g.*, milk and other dairy products, eggs, pet food) to increase the protein content according to Kjeldahl method-based protein analysis by unethical manufacturers.[2] In the past, food recalls were triggered by the discovery of melamine in products, and a major incident occurred in 2008 when high levels were found in milk and baby formula, causing serious health problems,[3] such as the formation of insoluble melamine cyanurate crystals in the kidneys, thus causing renal failure. Ingestion of melamine at levels above the safety limit (2.5 mg L^{-1} in the USA and the UK; 1 mg L^{-1}

[a] *Department of Chemistry, Birla Institute of Technology and Science Pilani, Hyderabad campus, Hyderabad, Telangana, 500078, India. E-mail: nilanjandey.iisc@gmail.com, nilanjan@hyderabad,bits-pilani.ac.in*
[b] *Michael Smith Laboratories, University of British Columbia, Vancouver V6T 1Z4, Canada*

† Electronic supplementary information (ESI) available. See DOI: https://doi.org/10.1039/d5ma00470e

for infant formula in China) can induce renal failure and even death in pets and infants.[4] To protect people, especially infants, strict limits have been set on how much melamine can be allowed in food. This makes it important to develop easy and accurate ways to detect melamine in food products to ensure safety. However, most of the sensors reported to date for melamine fail to achieve quantitative detection due to background interference, non-linear optical response, cross-reactivity, *etc.*

In such cases, integration of machine learning-based algorithms to analyse the data set obtained from traditional solution-based techniques would be particularly interesting, as they can improve the analytical efficacy of the system by enhancing the sensitivity of probe molecules, accuracy, and real-time processing *etc.* ML algorithms manage large datasets, filter noise, and improve analyte detection in complex environments, making them crucial for environmental monitoring and diagnostics applications. ML-driven sensors offer predictive analysis and personalized solutions, while also reducing costs and optimizing design, establishing machine learning as a key force in developing scalable, efficient sensing technologies.[5] Furthermore, the incorporation of polyaromatic scaffolds into the molecular backbone will result in building up self-assembled architectures. These moieties, through non-covalent interactions such as hydrophobic interactions or π–π stacking, guide the self-assembly of molecules into ordered structures. The extent of self-assembly can affect the morphology of the materials, surface area, and arrangement of functional groups, directly enhancing the sensing efficiency by improving signal transduction and analyte recognition.[6] Also, it has often been observed that probe molecules in close-packed self-assembled structures can provide a suitable binding cleft for target analytes through multipoint interactions.[7]

In this paper, we have designed two easily-synthesizable pyrimidine derivatives with polyaromatic scaffolds, namely anthracene and pyrene, as signalling moieties that can form self-assembled nanostructures in an aqueous medium. It was found that both compounds showed ''turn-on'' fluorescence response exclusively in the presence of melamine, presumably through the formation of a complementary hydrogen bonding network.[8] Despite such similarities, the degree of response (sensitivity of the system) was found to be dependent on the electronic nature, conformation and self-assembly behavior of the probe molecules.

Upon spectroscopic investigation, we would like to utilize this system for the determination (detection and quantification) of melamine in various real-life samples (milk and other milk products). Additionally, we aim to develop chemically modified coated paper strips for on-site detection of melamine.

Results and discussion

Design and synthesis of the probe molecule

In the present work, we have synthesized two pyrimidine-based fluorogenic amphiphiles, featuring distinct donor units, namely pyrene (**1**) and anthracene (**2**) (Fig. 1a).[9] Both compounds were thoroughly characterized by ^{1}H NMR, and FT-IR spectroscopy (S1, ESI†).

The presence of polycyclic aromatic scaffolds such as pyrene and anthracene improves the self-assembly properties of the molecules *via* π–π stacking and hydrophobic interactions. Moreover, these moieties are known for their susceptibility to the microenvironment. Changes in local pH, temperature, viscosity, *etc.* can affect the degree of aggregation, as noted by the distinct monomer-to-excimer ratio. The incorporation of the pyrimidine unit in the molecule is crucial as it can form a long-range supramolecular architecture *via* extensive donor–acceptor type complementary hydrogen bonding interaction.

Moreover, connecting such electron-deficient pyrimidine units with electron-rich pyrene/anthracene moieties will enhance charge transport within the molecular framework, leading to improved sensing performance.

Computational details for both compounds

Both compounds **1** and **2** were energy-optimized using the B3LYP level of theory with a 6-31G* basis set in the gas phase. The structure of **1** showed a nearly planar structure with a dihedral angle of $\sim 0.2^\circ$ between the pyrimidine unit and pyrene moiety, whereas for compound **2**, the dihedral angle between the anthracene and pyrimidine unit was found to be $\sim 50.8^\circ$. This indicated that compound **2** has a more twisted conformation than that of **1**.[10] This conformational difference can be ascribed to the steric repulsion of anthracene aromatic protons with adjacent carbonyl groups and the olefinic proton of the pyrimidine moiety.[11] Such differences in conformation are expected to lead to the formation of distinct self-assemblies through varied levels of stacking arrangements.

Furthermore, FMO (Frontier molecular orbital) analysis of compounds **1** and **2** indicated that the HOMO orbitals were mostly concentrated on the polyaromatic scaffolds (pyrene for **1** and anthracene for **2**), while the LUMO orbitals were located on the pyrimidine site along with donor moiety (Fig. 1c).[12] Such a kind of localization of FMOs at different parts of the probe molecules indicated the charge-transfer (CT) nature of the system, where the electron density can be transferred from the donor (pyrene or anthracene) to the acceptor (pyrimidine) moiety upon excitation.[13] The dipole moment of compound **1** (4.71 D) is found to be greater than that of compound **2** (2.78 D). The greater dipole moment in the pyrene-pyrimidine moiety implies a stronger interaction between the donor (pyrene) and acceptor (pyrimidine moiety).[14]

This can enhance the intramolecular charge transfer (ICT) properties, making the molecule more efficient in electronic and optical applications.[15] The electrostatic potential map (ESP) provides insights into the electron density distribution and identifies the most nucleophilic and electrophilic regions of the molecule. The blue-colored surface indicated a high electron density region, while the low electron density area was defined by a red-colored area. On the contrary, areas on the molecular surface where the enclosed negative electron charge and the positive core charge balanced each other (overall neutral charge), are mostly designated by green. From this,

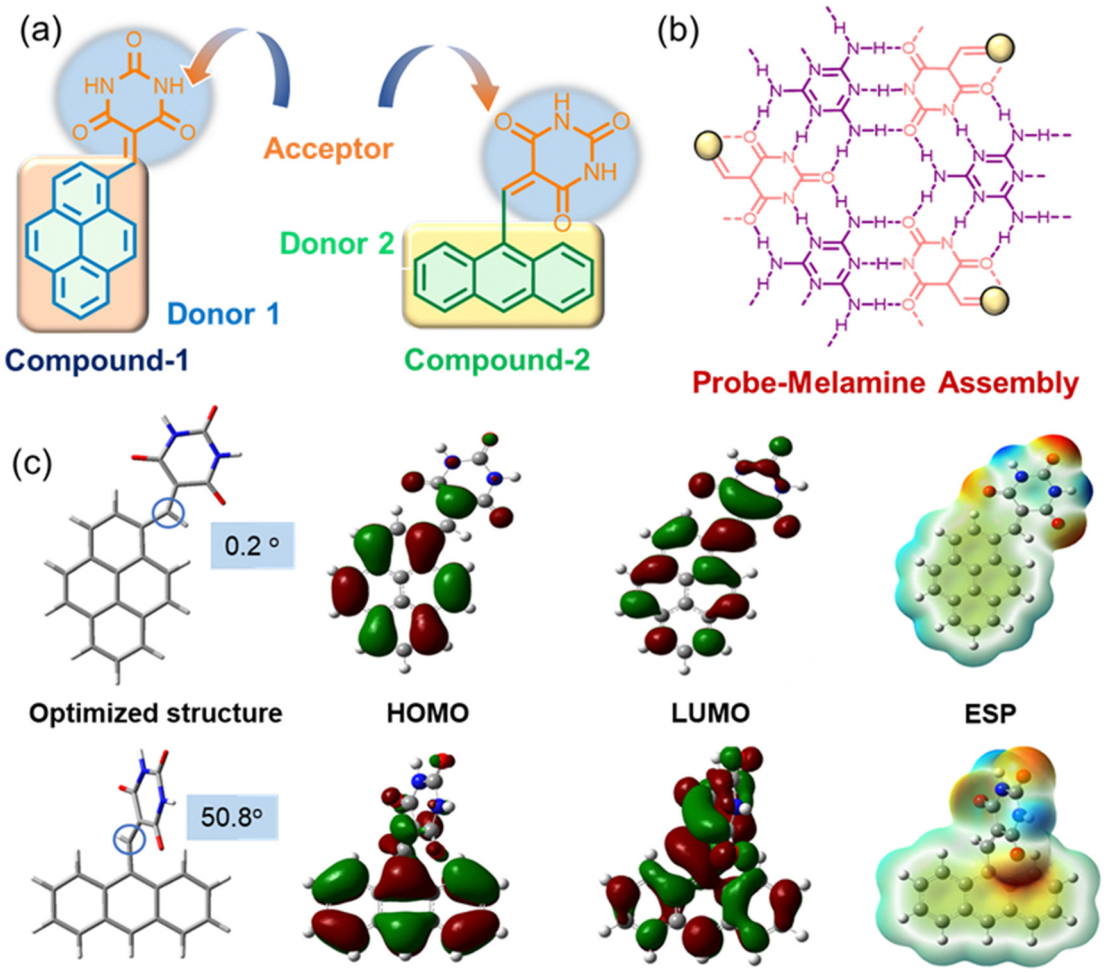

Fig. 1 (a) Chemical structures of compounds **1** and **2**. (b) Schematic diagram showing self-assembly of the compounds with melamine. (c) Energy minimized structures of compounds **1** and **2** with MEP (molecular electrostatic potential) surfaces and Frontier orbital analysis (B3LYP/6-31G* level).

we can conclude that the carbonyl groups (C═O) present in the pyrimidine units are electron-deficient and act as hydrogen bond acceptors, while the –NH groups are electron-rich, serving as hydrogen bond donors.[16]

Photophysical and aggregation properties

The fluorescence spectra of compound **1** were recorded across a wide range of organic solvents and water media. In aprotic organic solvents (both polar and nonpolar), the compound showed highly structured fine spectra with maxima at ~385 and 410 nm. Along this, a small hump was observed at 430 nm (Fig. 2a). However, in protic solvents, such as methanol, ethanol, and water, we witnessed a broad red-shifted fluorescence spectrum. The degree of red-shift as well as the emission intensity of this broad band depends on the hydrogen-bonding ability of the solvent. From ethanol to methanol to water, we noted a red-shift in emission maxima with substantial quenching in emission intensity (Fig. 2b). We believe that in protic solvents, the compounds form larger aggregated species through hydrogen bonding as well as π-stacking interactions, which is evident by the relative ratios of monomer *vs* aggregated emission. The bathochromic (red) shift in the emission bandwidth with an increase in polarity indicates that the excited state of compound **1** is more polarised than the ground state, which is a consequence of the ICT process.[17]

The UV-visible spectra of compound **1** exhibited two distinct absorption bands in the 365 (2×10^4 M^{-1} cm^{-1}) and 440 nm (4×10^4 M^{-1} cm^{-1}) regions in a THF medium, while in the aqueous medium, compound **1** experienced a hypochromic shift with substantial broadening (Fig. 2d). Notably, residual absorbance observed in the longer wavelength region was presumably due to the Mie scattering effect, caused by the presence of colloidal nanoscopic aggregates in the water medium. Additionally, the red-shifted absorption maxima (470 nm) in the aqueous medium indicated the charge-transfer nature of the aggregates, induced by hydrogen bonding interactions.[18,19]

Excitation spectra were recorded at both the 385 nm and 472 nm emission maxima in a water medium, revealing a distinct signature, indicating the presence of at least two different photoactive ground state species[20] (Fig. 2c). The spectrum corresponding to the 385 nm emission band appeared broad and blue-shifted compared to the excitation spectrum at the 472 nm emission band. The excitation spectra correspond to the 385 nm emission band, resembling the excitation spectrum of the

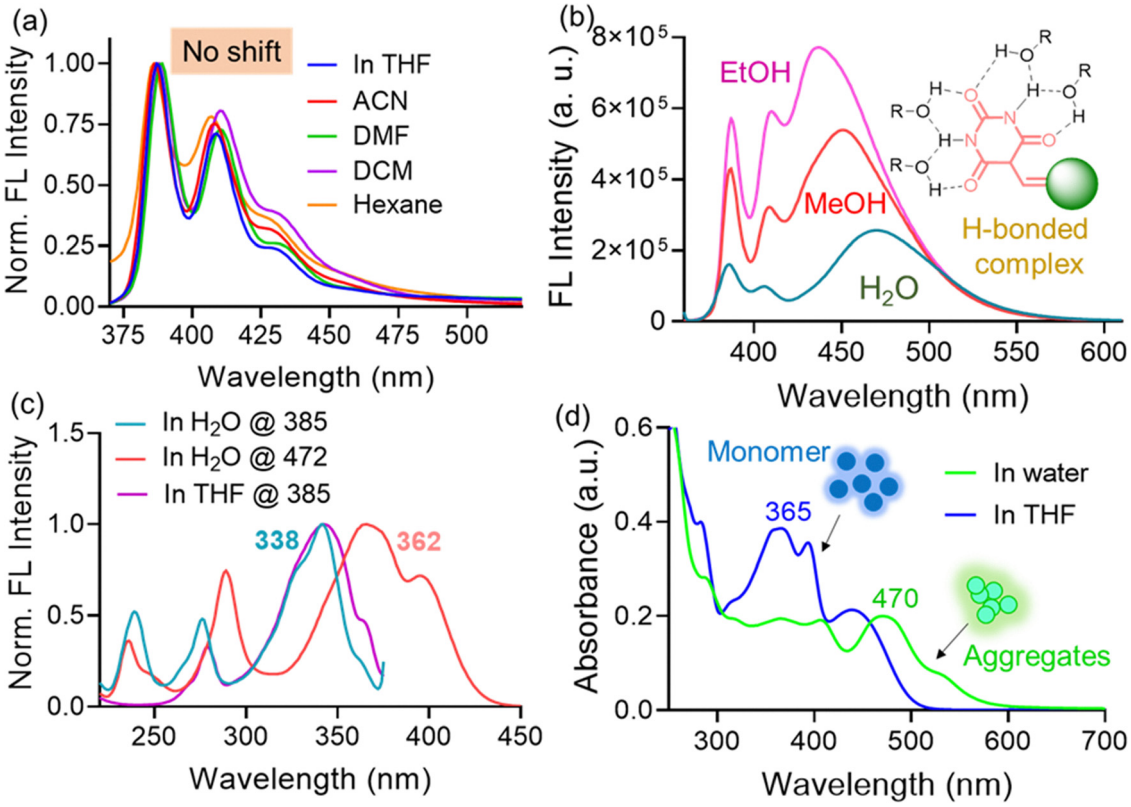

Fig. 2 Fluorescence spectra of **1** (10 μM, λ_{ex} = 350 nm) in (a) polar aprotic solvents (normalised) and (b) polar protic solvents. (c) Fluorescence excitation spectra of **1** (both at 385 and 472 nm emission bands) in THF and water medium. (d) UV-visible spectra of **1** (10 μM) in THF and water medium.

compound observed in the THF medium. This indicated that the emission band centered at 385 nm could have originated from monomer species. Thus, it can be argued that the broad and red-shifted peak observed at ~472 nm could be assigned to aggregated species.[21,22]

The dynamic light scattering experiment suggested that compound **1** formed aggregates with an average hydrodynamic diameter of 308 ± 5.8 nm in the aqueous medium (Fig. 3c), while the analysis of the FE-SEM images indicated oval-shaped morphology (Fig. 3c inset). Additionally, time-correlated single-photon counting (TCSPC) experiments were conducted for compound **1** in both water and THF medium to understand the stability and decay kinetics of excited-state photoactive species (Fig. 3d). In the THF medium, compound **1** exhibited multi-exponential decay with an average lifetime of 5.66 ns, while in the water medium, it showed a relatively shorter lifetime (3.88 ns). This shorter decay time could be attributed to the formation of π-stacked self-assembled structures in the aqueous medium.[23]

The pH and thermoresponsive properties highlight the sensor's environmental sensitivity, making it suitable for use in varied sample conditions and offering tunable performance in real-world applications. A temperature-variation study of compound **1** in the aqueous medium showed an enhancement of fluorescence intensity along with a 5 nm blue shift in emission maxima (Fig. 3a). This could be attributed to the association of aggregates, induced by thermal agitation at high temperatures.[24] At high temperature, there could be a change in the nature of the aggregates due to the dissociation of the hydrogen-bonding network. The π-stacked self-assemblies, formed *via* hydrophobic interactions at high temperatures, showed enhancement of excimer emission. Additionally, the blue-shifted maxima observed at elevated temperature indicated a hydrophobic microenvironment around the probe molecules. Fluorescence spectra of compound **1** at different pH conditions exhibited distinct features (Fig. 3b). At acidic pH (pH 4), the pyrimidine unit is protonated, which promotes intermolecular hydrogen bonding and π–π stacking of the pyrene units. This leads to increased aggregation and consequently, a higher intensity of the aggregation band relative to the monomer band. As the pH increases to neutral (pH 7.4), partial deprotonation occurs, reducing hydrogen bonding and aggregation. This results in a relative increase in the monomer emission band, reducing the prominence of the excimer band. At basic pH (9.4), complete deprotonation introduces significant electrostatic repulsion, disrupting aggregation and stabilizing the monomeric form. This leads to a further increase in the monomer emission band relative to the aggregation band. Thus, it could be concluded that the changing microenvironment (pH and temperature) showed a significant influence on the aggregation of compound **1**.[25]

Interaction with melamine

The presence of complimentary hydrogen bonding motifs intrigued us to investigate the interaction of compound **1** with

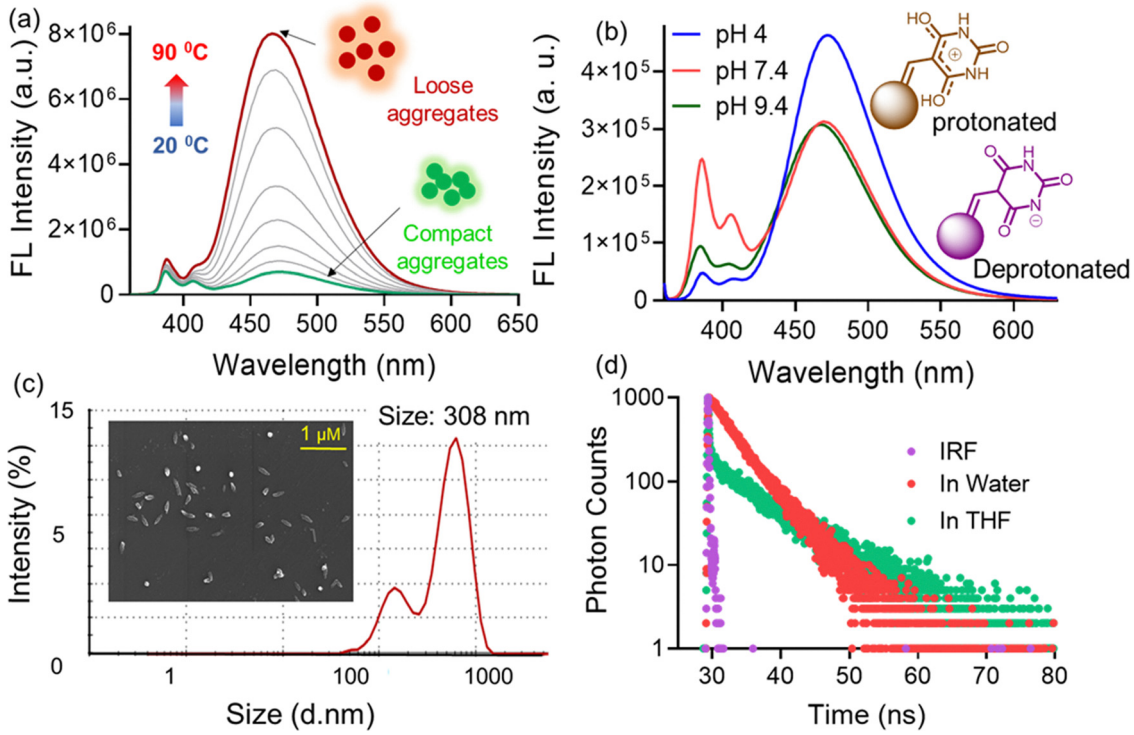

Fig. 3 Fluorescence spectra of **1** (10 μM, λ_{ex} = 350 nm) at different (a) temperatures and (b) pH in the aqueous medium. (c) FE-SEM image (inset) and DLS data for the compound **1**. (d) Fluorescence decay profile of **1** (10 μM) in the THF and water medium.

melamine in the aqueous medium.[26] The small quenching observed in the UV titration (Fig. S3, ESI†) suggests that the interaction between melamine and pyrene-barbituric acid is insufficient to significantly alter the electronic transitions of the pyrene moiety. Adding melamine to the aqueous solution resulted in the appearance of blue fluorescence under a long UV lamp (Fig. 4b inset). As expected, the fluorescence spectrum with melamine showed a turn-on response at the aggregated emission band, while less change in emission intensity was noted at the monomer band. Furthermore, fluorescence titration studies were performed with melamine (0–400 μM) under similar conditions (Fig. 4b). With increasing melamine concentration, the emission intensity at the 470 nm band gradually enhanced. A ~2.0-fold increment was noted upon the addition of ~400 μM of melamine. Also, the titration studies indicated that the present system can detect melamine as low as 0.8 ppb in the aqueous medium.

Interestingly when the same amount of melamine was added to compound **2** the band at 470 nm was increased approximately 5-fold (Fig. 5d). Compound **2** shows a better response (approximately 4 times) as compared to compound **1** (Fig. 5c). This may be attributed to a different conformation as compared to pyrene, which allows it to have stronger interactions with melamine through π–π stacking. This enhances the efficiency of energy transfer, leading to a more noticeable fluorometric change.[27,28] Given that selectivity is crucial in real-life sample analysis, the response of compound **1** to other competitive analytes was also examined (Fig. 4d). The extents of interaction with other analytes, as defined by changes in FL intensity at the 470 nm band, were found to be significantly less compared to melamine. The enhanced selectivity arises primarily from the complementary hydrogen bonding interactions between the pyrimidine unit of the probe and the triamine structure of melamine. Specifically, melamine contains three exocyclic –NH_2 groups capable of acting as both hydrogen bond donors and acceptors, which align precisely with the C═O and –NH groups of the pyrimidine scaffold to form stable, directional, and multivalent hydrogen-bonded assemblies. In contrast, common milk components such as sugars (*e.g.*, lactose, glucose, *etc.*) primarily form weak hydrogen bonds with –OH groups, lacking the defined geometry and complementarity required for strong probe-analyte complexation. Proteins are too large and structurally complex, with interactions that are often sterically hindered and non-specific. This indicated the robustness of the present system in estimating melamine in real-life samples. In the time-correlated single-photon counting (TCSPC) experiment, the average fluorescence lifetime of compound **1** monitored at 470 nm increased from 3.88 to 3.93 ns in the presence of melamine (Fig. 4c). This nearly unchanged lifetime suggests that the intrinsic deactivation pathways, both radiative and non-radiative, of the excited state remain largely unaffected after the addition of melamine.[29]

To evaluate the effects of the local surroundings, we have examined the sensing efficacy of the probe molecules at different temperatures and pH conditions. pH variation studies revealed that at a neutral pH (7.4), the maximum change was observed after the addition of melamine (Fig. 4a), though melamine-driven changes in fluorescence signal were observed

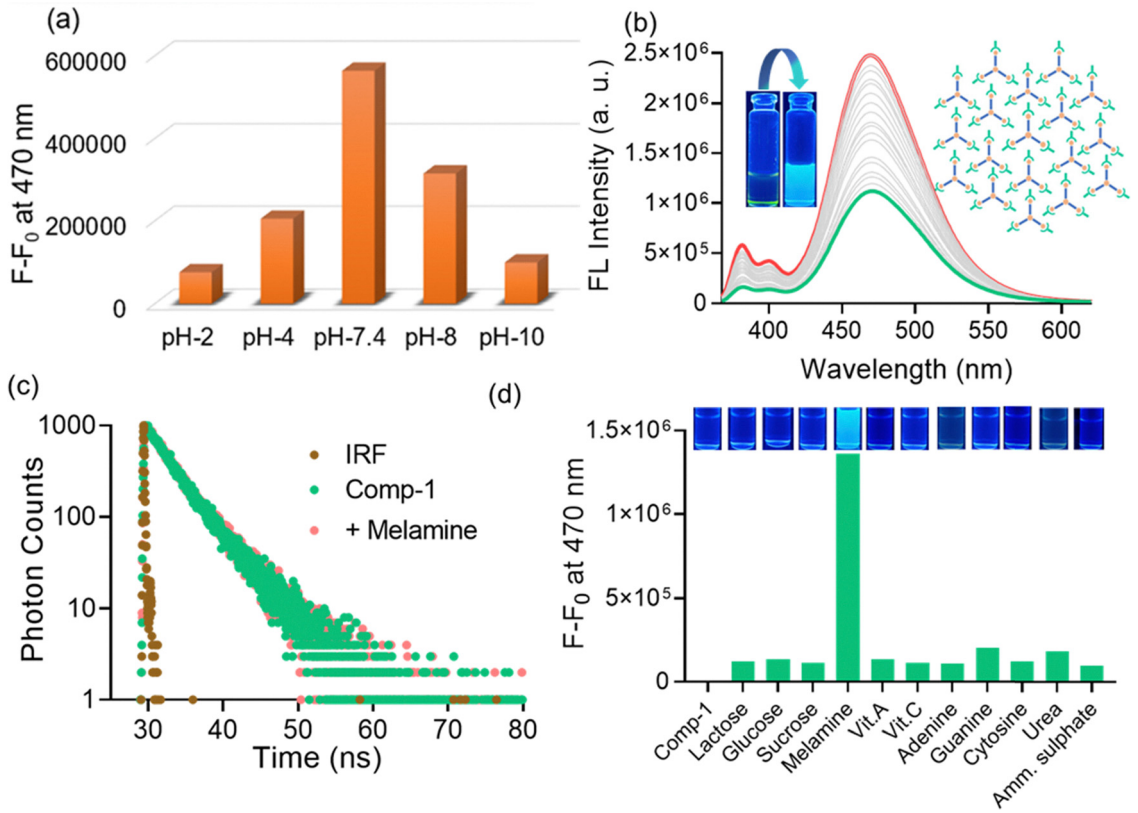

Fig. 4 Change in fluorescence intensity of **1** (10 μM, λ_{ex} = 350 nm) at 470 nm upon the addition of (a) melamine (400 μM) in different pH medium and (d) different analytes (400 μM) in an aqueous medium. (b) Fluorescence titration of **1** (10 μM, λ_{ex} = 350 nm) with melamine (0–400 μM) in an aqueous medium. (c) Fluorescence decay profile of **1** (10 μM) before and after the addition of melamine (400 μM) at 470 nm.

in a wide range of pH (2–10), the maximum response was noticed at neutral pH conditions (6–8), because at neutral pH, both the melamine and pyrimidine moiety are in their optimal protonation states, facilitating efficient hydrogen bonding.[30]

This results in stabilized excited states and an enhanced fluorescence response. Probably at extreme pH conditions (basic as well as acidic), the shift in tautomeric equilibrium diminishes the hydrogen bonding efficiency of the pyrimidine unit, leading to a mild response towards melamine. To determine the stability of the hydrogen-bonded adduct with melamine, we recorded the fluorescence spectra at different temperatures (20 °C to 90 °C) in the aqueous medium (Fig. S4, ESI†). With an increase in temperature the intensity at the excimer band increases; this may be attributed to the partial weakening of hydrogen bonds between the melamine and pyrimidine residues, which might reduce the rigidity of the system.[31] This increased flexibility could promote aggregation of the pyrene units, enhancing excimer formation.

Regression analysis for predicting normalized intensity of melamine

In this study, various machine learning models have been utilized to predict the normalized intensity of melamine based on concentration *vs.* intensity data. Our dataset began with 20 data points representing the relationship between melamine concentration and its corresponding normalized intensity. To enhance the robustness of our model, we employed a data augmentation technique, generating an additional 10 000 synthetic data points by interpolating between the minimum and maximum values of the original dataset.

Out of many regression algorithms, we have selected support vector regression (SVR) with both linear and quadratic kernels, linear regression, and AdaBoost regression. The rationale for choosing these models stems from their diverse capabilities to capture complex relationships in the data. SVR, in particular, is adept at handling non-linear interactions commonly observed in spectroscopic data.[32] Each model was trained on the augmented dataset, with the training process involving fitting the models to the synthetic intensity data derived from the concentration values. We evaluated the performance of these models using several statistical metrics, including mean squared error (MSE), coefficient of determination (R^2), and root mean squared error (RMSE).[33]

Formula for mean squared error (MSE) $\frac{1}{n}\sum_{i=1}^{n}(y_i - \hat{y}_i)^2$

Formula for root mean squared error (RMSE) $\sqrt{\frac{1}{n}\sum_{i=1}^{n}(y_i - \hat{y}_i)^2}$

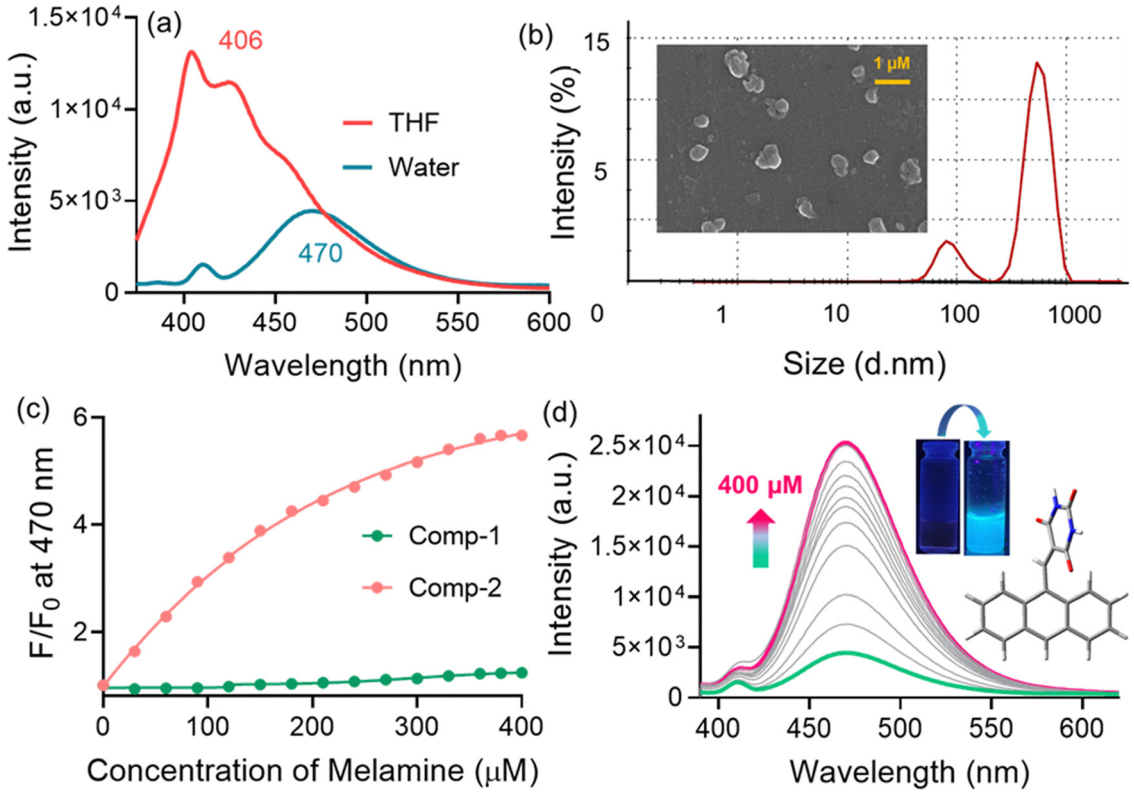

Fig. 5 (a) Fluorescence spectra of **2** (10 μM) in THF and water medium. (b) FESEM image (inset) and DLS data for compound **2**. (c) Change in fluorescence intensity of **1** and **2** at 470 nm upon adding melamine (400 μM) in an aqueous medium. (d) Fluorescence titration of **2** (10 μM, λ_{ex} = 360 nm) with melamine (0–400 μM) in an aqueous medium.

Formula for coefficient of determination (R^2) $1 - \frac{\sum_{i=1}^{n}(y_i - \hat{y}_i)^2}{\sum_{i=1}^{n}(y_i - \bar{y})^2}$

Table 1 Performance of models using several statistical metrics, including mean squared error (MSE), coefficient of determination (R^2), and root mean squared error (RMSE)

Method	Mean squared error	Root mean squared error	*R*-squared
SVR linear	0.0042	0.0649	0.9724
Linear regression	0.0006	0.0249	0.9959
SVR quadratic	0.0103	0.1015	0.9326
AdaBoost regression	0.0008	0.0295	0.9942

These metrics provide quantitative assessments of the model's predictive accuracy, with lower values indicating superior performance as shown in Table 1.

To visualize the predictive capabilities of each model, we generated plots of actual *versus* predicted intensity values. These plots depicted the relationship between the observed and predicted intensities, complete with regression lines that illustrate the model fit to the data. The analysis revealed varying degrees of accuracy, with SVR quadratic (Fig. 6c) and AdaBoost regression (Fig. 6d) consistently demonstrating the best performance in predicting normalized intensity.

The linear regression model (R^2 = 0.9959) stands out with the best performance metrics (Fig. 6b), reinforcing that a linear approach is highly effective for predicting normalized intensity based on concentration in this dataset.[34] The simplicity and interpretability of linear regression make it the most suitable model given the strong linear relationship. The other models (Fig. 6a), while also performing well, do not surpass the linear model's effectiveness, and more complex models like SVR quadratic (Fig. 6c) may introduce unnecessary complexity without providing significant benefits.

By employing machine learning techniques in this research, we underscore the significant potential for these methodologies to enhance predictive analysis in chemical sensing applications. Our findings contribute to the growing body of literature highlighting the effectiveness of advanced computational methods in analytical chemistry, particularly in accurately predicting intensity linked to melamine concentration.

Mode of interaction between the probe and melamine

A series of spectroscopic experiments was conducted to elucidate the precise mode of interaction between compound **1** and melamine. The FT-IR spectra of compound **1** before and after the addition of melamine indicated a shift in the C=O (of pyrimidine unit) stretching frequency to the lower energy

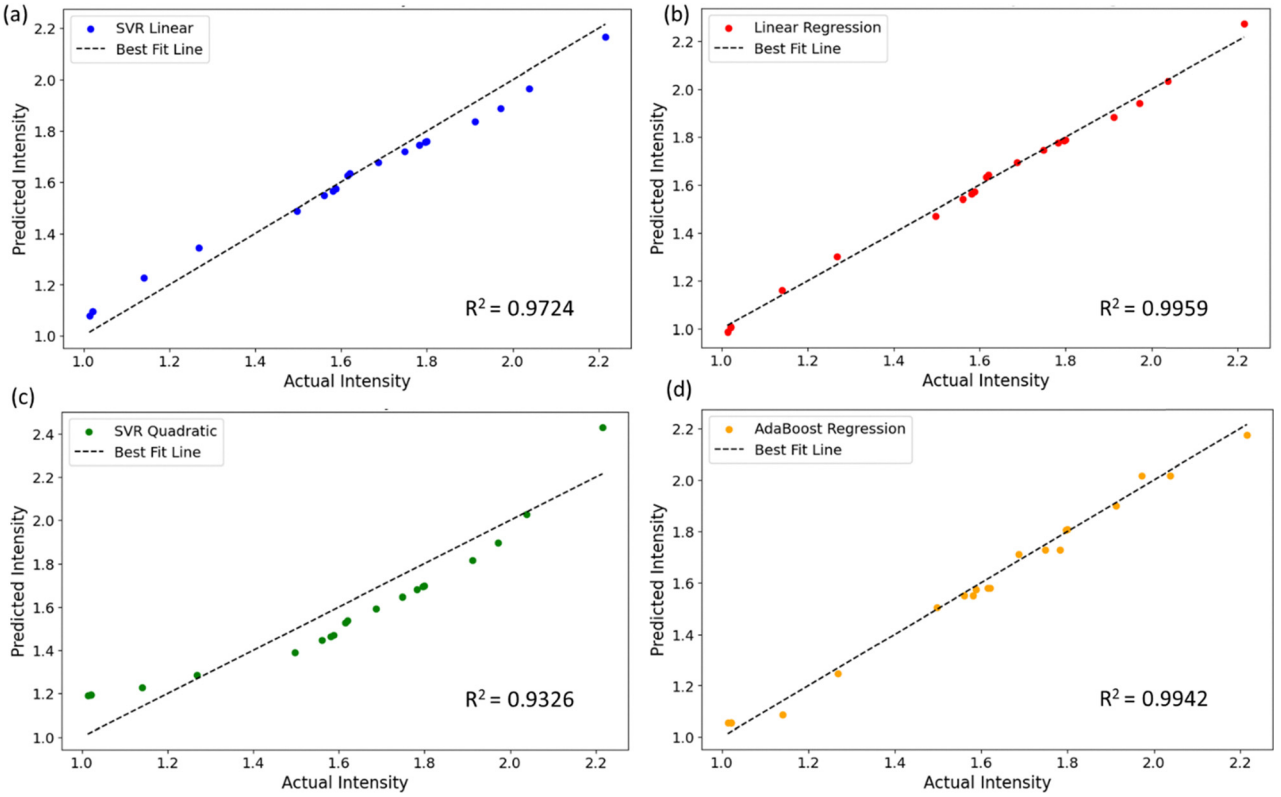

Fig. 6 (a) Plots of actual *versus* (Fig. 1) predicted intensity values of (a) SVR linear, (b) linear regression, (c) SVR quadratic, and (d) AdaBoost regression.

region, from 1728 to 1660 cm^{-1} (Fig. 7e), which indicated the formation of hydrogen bonds with melamine –NH units. Additionally, hydrogen bonding interaction involving the pyrimidine–NH group was also evident from FT-IR analysis, as the corresponding stretching band (3390 cm^{-1}) became broad.[35,36] Though all the spectroscopic studies were performed in an aqueous medium, we have conducted ^{1}H-NMR studies in DMSO-d_6 due to the limited solubility of the probe molecules in D_2O. The ^{1}H NMR spectra of compound **1** with melamine in DMSO-d_6 were recorded to further investigate the interaction mode between the probe and melamine (Fig. 7b). The peak labelled as 'a' shifted from 9.1 ppm to 10.6 ppm, and the protons labelled as 'b' and 'c' nearly disappeared upon interaction with melamine. This is indicative of hydrogen bonding interactions between melamine and the pyrimidine moiety.[37]

As expected, the aromatic proton adjacent to the pyrimidine moiety exhibited a downfield shift from approximately 8.4 to 8.6 ppm upon interaction with melamine, indicating a change in the chemical shift due to the formation of a complex. In contrast, the protons located farther from the pyrimidine unit did not display significant shifts, suggesting minimal change in their environment. Additionally, upon the addition of melamine, the –NH resonances at around 11.2 and 11.5 ppm were no longer observed, likely due to hydrogen bonding interactions between the pyrimidine residue and melamine, which resulted in the disappearance of these signals.[38,39]

To evaluate the hydrogen-bonding interaction between the probe and melamine, we examined the interaction of the compound with melamine in the presence of a known chaotropic agent, urea. The fluorescence response of compound **1** towards melamine was reduced significantly in the presence of 5 M urea (Fig. 7d). This observation could indirectly prove the essential role of hydrogen bonding interactions in the formation of supramolecular co-assembly with melamine (Fig. 1b).[40]

Additionally, dynamic light scattering (DLS) experiments revealed the formation of larger colloidal particles with an average diameter of 638.2 ± 5.7 nm in the presence of melamine (Fig. 7c). Consequently, FESEM images of the **1** melamine adduct displayed larger spherical aggregated structures (Fig. 7c inset). Changes in aggregation were also evident from FL-lifetime analysis. These spectroscopic results suggest that the formation of hydrogen bonds between compound **1** and melamine leads to notable changes in both the IR and NMR spectra, providing strong evidence for the mode of interaction and the resultant supramolecular assembly formation, which is responsible for the observed turn-on fluorescence response (Fig. 7a).

MD simulations with both the probes

MD simulations with compounds **1** and **2** were performed for 120 ns with 10 molecules in each case (Fig. 8a and b). Both compounds showed self-assembly formation with time. The self-assembled structures of **1** after 120 ns showed an anti-parallel arrangement with the pyrene moiety of one molecule π-stacked with the pyrimidine unit of another molecule. On the contrary, in the case of compound **2**, anthracene moieties were

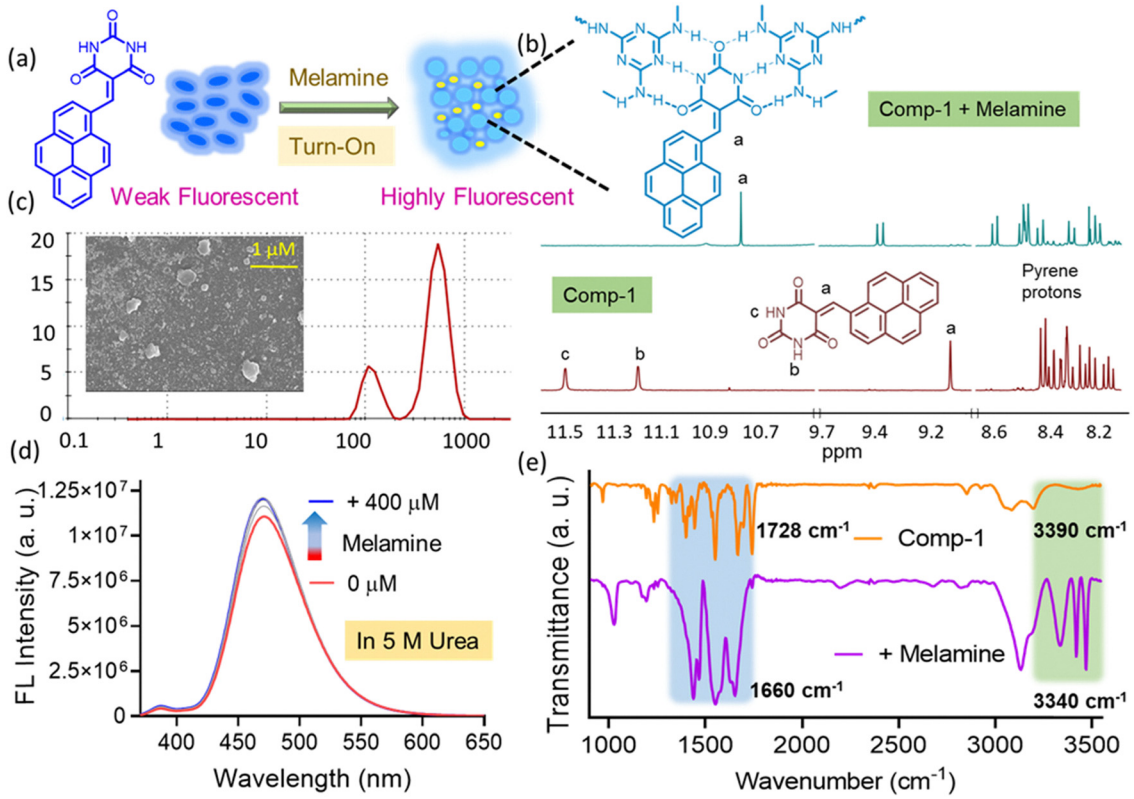

Fig. 7 (a) Schematic showing the aggregation after the addition of melamine in compound **1**. (b) Partial ^{1}H-NMR spectrum of **1** (5 mM) with melamine (2 equiv.) in DMSO-d6 medium. (c) FESEM image (inset) and DLS data for the **1**.melamine (**1** = 10 μM, melamine = 400 μM) conjugate. (d) Fluorescence titration of **1** (10 μM, λ_{ex} = 350 nm) with melamine (0–400 μM) in a 5 M urea solution. (e) FT-IR spectra of **1** and **1**.melamine.

involved in face-to-face π-stacking interaction, while multiple hydrogen bonds (1.8–2.2 A°) were observed among pyrimidine residues. The number of hydrogen bonds increased with self-assembly formation, especially for compound 2 (Fig. 8e).[41] This observation corroborated with the spectroscopic findings, where we observed a larger excimer-*vs*-monomer emission for

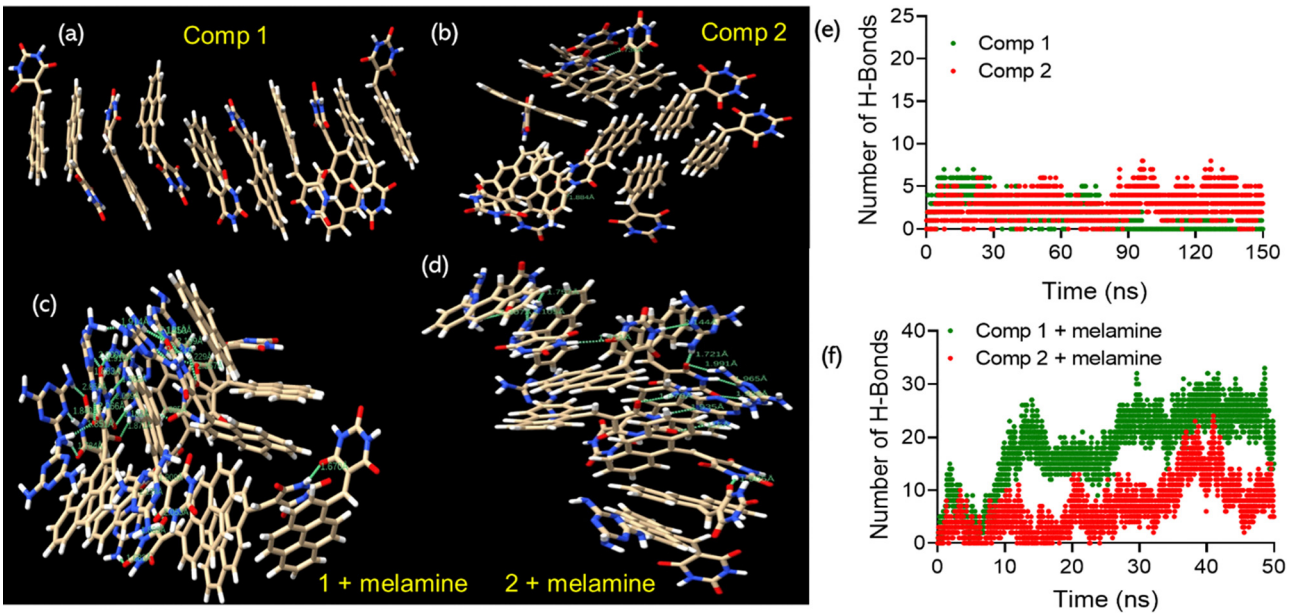

Fig. 8 Self-assembled structures of (a) compounds **1** and (b) **2** after 120 ns and the corresponding melamine composites (c) and (d) after 40 ns. Number of hydrogen bonds present in the self-assembly of compounds **1** and **2** (f) with and (e) without melamine over time.

compound **2**. However, both the electrostatic (7210.33 kJ mol^{-1} for **1** and 7014.16 kJ mol^{-1} for **2**) and van der Waals interaction energies (−701.31 kJ mol^{-1} for **1** and −539.48 kJ mol^{-1} for **2**) between molecules of **1** were found to be larger than those of **2**. The larger electrostatic interaction energy for the self-assembly of **1** indicated more charge transfer (CT) characteristics, which might be attributed to the proximity of the pyrene units and pyrimidine residues. Compound **1** in the aqueous medium showed a relatively fast decay profile with an average excited state lifetime of 3.88 ns, which was slower for compound **2** (3.45 ns). This again confirmed the CT nature of the aggregates for compound **1**. The higher van der Waals (VdW) interaction energy for compound **1** suggested a better packing arrangement or closer molecular proximity in the self-assembled state.[42] This observation also aligned with the experimentally observed DLS data. The average hydrodynamic diameter for compound **1** was found to be smaller than that of **2**, which suggested the compact packing of the molecules in the aggregated state. However, the negative values of VdW energy in both cases indicated an attractive force between the molecules, contributing to the stabilization in the self-assembled state.

Furthermore, we attempted to study the interaction of **1** and **2** with melamine. In both cases, the addition of melamine resulted in more aggregated structures with the presence of a greater number of hydrogen bonds (Fig. 8c and d).

The polyaromatic residues were found to be in close proximity, which could lead to an increase in the excimer emission. This was also supported by experimental observation, where we witnessed a turn-on fluorescence response for both **1** and **2** upon the addition of melamine. A closer view indicated that the pyrene units in **1**.melamine assembly mostly preferred the slipped conformation. At the same time, the anthracene moieties in the case of **2** showed a well-π-stacked conformation, though some conformations are T/L-shaped. The larger fluorescence response (F/F_0) for compound **2** with melamine might be attributed to such differences in the arrangements of the polyaromatic residues in the aggregated state. The average number of hydrogen bonds in the case of **1** was found to be ∼22–25 after 50 ns, which appeared to be ∼12–15 for compound **2** (Fig. 8f). These hydrogen bonds were mostly observed between the pyrimidine residues and melamine units. The differences in the conformations of compounds **1** and **2** (planar *vs.* twisted) might be one of the contributing factors to dictate the hydrogen bonding interaction with melamine.[43] A significant reduction in the electrostatic interaction energy for both **1** (−411.42 kJ mol^{-1}) and **2** (−158.48 kJ mol^{-1}) in the presence of melamine suggested that the self-assembly formation was mostly dominated by hydrogen bonding and π-stacking interaction. Also, smaller VdW energy values (−163.73 kJ mol^{-1} for **1** and −102.18 kJ mol^{-1} for **2**) observed in both cases suggested the formation of large-sized aggregates with the addition of melamine, which was also confirmed by the DLS experiment.

Impact of signalling moiety on analytical performance

Compounds **1** and **2** share an identical binding site for melamine; however, they exhibit distinct responses upon interaction with the melamine. To understand this variation in sensing behavior, we systematically investigated the influence of the signalling moiety on the analytical performance of the probe molecules.

The UV-visible spectra of compounds **1** and **2** in an aqueous medium exhibit distinct absorption features corresponding to their electronic transitions (Fig. S2, ESI†). A broad absorption band centered around 470 nm for compound **1** is indicative of an n–π* transition, while for compound **2**, this band appears at approximately 440 nm. The observed 30 nm blue shift in compound **2** can be attributed to its less extended π-conjugation system compared to the planar structure of pyrene in compound **1**.[44]

As already discussed, compound **2** adopts a twisted molecular conformation, whereas compound **1** assumes a planar arrangement. This structural difference significantly influences their self-assembly behavior, as demonstrated by dynamic light scattering (DLS) and field-emission scanning electron microscopy (FE-SEM) analyses (Fig. 5b). The DLS studies showed the formation of particles with a larger hydrodynamic diameter (485.7 ± 18.2 nm) for compound **2** than that of compound **1**. Compound **2** exhibits a higher degree of aggregation than compound **1**, which can be attributed to its twisted molecular arrangement, promoting enhanced intermolecular interactions and aggregation. The difference in the charge transfer for both compounds also results from the difference in the dihedral angle.[45] The fluorescence spectra of compound **2** in THF and aqueous medium display similar features to those observed for compound **1** (Fig. 5a). In THF, compound **2** exhibits characteristic monomer emission, indicative of its molecularly dispersed state. In contrast, in an aqueous medium, compound **2** demonstrates fluorescence associated with aggregation, consistent with the behavior observed for compound **1**. In the time-correlated single-photon counting (TCSPC) experiment, the average fluorescence lifetime of compound **1** monitored at 470 nm is 3.88 ns, and for compound **2** the average lifetime is around 3.45 ns (Fig. S5, ESI†). This extended lifetime may be attributed to the enhanced aggregation of compound **2** in the aqueous medium.

Overall, the distinct conformation, extended conjugation, and charge transfer in the probe molecules result in different analytical performances for the melamine.

Estimation of melamine in milk products

Melamine contamination in milk products, particularly infant formula and milk powder, poses a significant health risk, especially to infants. The FDA safety limits for melamine are 20 μM for milk and 8.0 μM for infant formula.[46] Exceeding these limits can lead to serious health consequences, including kidney damage and other toxic effects, particularly in vulnerable populations like infants. Given the strict regulatory limits on melamine levels in food, there is a critical need for reliable, rapid, and cost-effective detection methods.[47] Therefore, it is essential to devise a reliable analytical method to verify even a minimal change in melamine level in milk and other dairy products. Considering these facts, we have employed probe **1** to

estimate melamine in milk samples. To validate the proposed method to specifically detect melamine in raw milk, known quantities of melamine were spiked into the milk samples. Before spiking melamine into milk and milk product samples, a pre-treatment step involving chloroacetic acid is essential. The addition of chloroacetic acid effectively destabilizes milk fats, which are subsequently removed *via* filtration. This removal is critical as residual fats can introduce turbidity or light scattering during spectroscopic analysis, potentially compromising the accuracy and reliability of the measurements. The acid treatment results in a clarified sample matrix suitable for precise analysis.

Furthermore, fluorescence spectral analysis revealed no significant changes in the emission profile of the probe molecule after the pre-treatment process. This observation confirms the absence of background interference attributable to the chloroacetic acid treatment, ensuring the integrity of the analytical procedure and the specificity of melamine detection in the treated milk samples.

The samples were prepared and analyzed according to the procedure as follows.[48] A 4.0 mL raw milk sample was placed into a 10 mL centrifuge tube, and 1.2 mL of 300 g L^{-1} trichloroacetic acid was added and mixed with a vortex for 5 min to deposit protein in the sample matrix. The mixture was centrifugated at 3500 rpm for 10 min. The supernatants were transferred into another centrifuge tube and adjusted to pH 7.4 with a small amount of 6 M NaOH, then filtered with a 0.22 μm filter. This filtrate was directly titrated with probe **1** for the detection of melamine (Fig. 9b). The fluorescence intensity of compound **1** at the 470 nm band increased with increasing volume of spiked milk samples (Fig. 9c). A nearly 2-fold increase in the emission intensity was observed at 470 nm after the addition of the 450 μM melamine spiked milk sample, which is almost in the same range as observed during titration studies. The minimum detectable concentration (LOD) of melamine was found to be less than the permissible limit. Calculations of percentage recovery values clearly stated that the present method could achieve a quantitative estimation of melamine.

This linear fluorescence response suggests that the present method could be utilized for quantitatively detecting melamine even in milk and other dairy products. Across all cases, the recovery values range between 96.2 and 105.7% with a relative standard deviation (RSD) of less than 5% (Fig. 9e). Furthermore, the same protocol was employed for the determination of melamine in other milk products such as milk powder and infant formula. In all cases, the estimated values were found to be in the same range as other reported values (Fig. 9d). Furthermore, the melamine content of each sample was also independently estimated by the LC-MS method.[49] An excellent agreement was observed between the values obtained from this method and the method described in this work (Table S1, ESI†).

A comparative overview of conventional melamine detection techniques, including their detection limits, analytical methods, and limitations, is provided in Table S2 (ESI†) to highlight the advantages of our ML-assisted fluorescent probe.

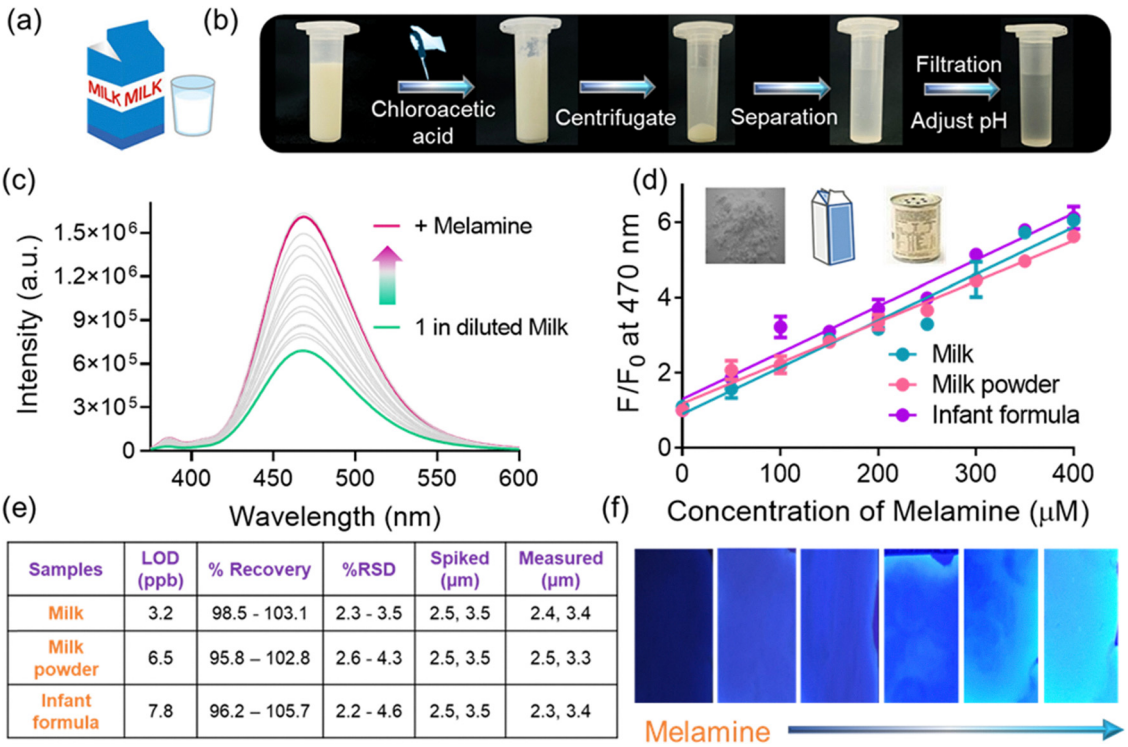

Samples	LOD (ppb)	% Recovery	%RSD	Spiked (μm)	Measured (μm)
Milk	3.2	98.5 - 103.1	2.3 - 3.5	2.5, 3.5	2.4, 3.4
Milk powder	6.5	95.8 – 102.8	2.6 - 4.3	2.5, 3.5	2.5, 3.3
Infant formula	7.8	96.2 – 105.7	2.2 - 4.6	2.5, 3.5	2.3, 3.4

Fig. 9 Schematic showing the (a) milk sample and (b) its pretreatment. (c) Fluorescence titration of **1** (10 μM, λ_{ex} = 350 nm) upon addition of milk extract (spiked with melamine). (d) Change in the fluorescence intensity of **1** with melamine (0–400 μM) in different milk products. (e) Quantitative analysis of melamine in different milk products. (f) Chemically modified paper strips with increasing amounts of melamine.

Low-cost paper strips for on-site detection of melamine

From the above discussion, it is evident that accurately measuring melamine in milk and other dairy products is crucial for quality control purposes. However, advanced laboratory facilities, as needed in traditional solution-based analysis, remain mostly unavailable in remote areas for rapid, on-location melamine detection. To address this, an alternative method using ''chemically modified paper strips'' was developed, which eliminates the need for complex instruments, tedious sample preparation, or specialized personnel.[50–52] The dye-coated paper strips showed no color under daylight while displaying a blue-colored fluorescence under a hand-held UV torch. The intensity of blue fluorescence was found to be dependent on the concentration of the probe molecule in solution as well as the emersion time. The stability of the paper strips was investigated under ambient conditions. No distinguishable changes in color intensity were observed when the paper strips were examined for 4–5 days at various time intervals. These results indicated the robustness of the paper strips and their suitability for the analysis of melamine. When the strips were subjected to different dosages of melamine, concentration-dependent enhancement of cyan-colored fluorescence was noticed (Fig. 9f). The image-J analysis indicated that the intensity of cyan-colored fluorescence was enhanced proportionately with the amount of melamine spiked. Since this procedure does not need any pretreatment of the samples or complex analysis of the output response, general people with limited knowledge would be able to perform it without much difficulty.

Conclusion

In this work, we designed and synthesized two pyrimidine-based probes with pyrene and anthracene donor substituents using a simple, scalable approach. Compound **1** exhibited aggregation in aqueous media but remained monomeric in THF and other aprotic solvents, while compound **2** adopted a twisted conformation (dihedral angle $\sim 50.85^{\circ}$) compared to the planar structure of compound **1** ($\sim 0.2^{\circ}$). In polar protic solvents (EtOH, MeOH, water), compound **1** formed pH-sensitive and thermoresponsive aggregates. Machine learning models were employed to predict normalized melamine intensity from concentration-dependent fluorescence data. The linear regression model (R^2 = 0.9959) showed the best accuracy, highlighting its suitability for this system. Both compounds showed turn-on fluorescence sensing of melamine, with a limit of detection (LOD) of 0.8 ppm. Spectroscopic studies confirmed that hydrogen bonding between the –C═O and –NH groups of the pyrimidine units and melamine's –NH groups altered the charge-transfer and aggregation behavior of the probes. The method was successfully applied for quantitative melamine detection in milk samples, with validation using alternative analytical methods.

Molecular dynamics (MD) simulations revealed that compound **1** forms anti-parallel π-stacked self-assemblies *via* pyrene–pyrimidine interactions, whereas compound **2** forms face-to-face anthracene stacking with multiple hydrogen bonds (1.8–2.2 Å) among pyrimidine residues, contributing to its enhanced stability. Additionally, we developed chemically modified paper strips for rapid, on-site melamine detection in milk. This portable method eliminates the need for complex instruments, making it accessible to non-specialists. Future efforts will focus on extending detection to other food adulterants and integrating the sensor into a user-friendly, portable device for field use.

Conflicts of interest

There are no conflicts to declare.

Data availability

The data will be available on reasonable request from the authors.

Acknowledgements

ND thanks Indian Council of Medical Research (ICMR) for the ITR grant (grant number: 2021-8350) and DST for the SYST grant (grant number: SP/YO/2021/1632) N. D. and HB thank BITS Pilani, Hyderabad campus for the financial and technical support. The authors also thank central analytical facilities BITS Pilani Hyderabad for the instrumental facilities.

References

1 O. J. Backhouse, J. C. Thacker and P. L. Popelier, A Re-evaluation of Factors Controlling the Nature of Complementary Hydrogen-Bonded Networks, *ChemPhysChem*, 2019, **20**(4), 555–564.
2 T. Steiner, The hydrogen bond in the solid state, *Angew. Chem., Int. Ed.*, 2002, **41**(1), 48–76.
3 K. Sharma and M. Paradakar, The melamine adulteration scandal, *Food Energy Secur.*, 2010, **2**(1), 97–107.
4 L. Li, B. Li, D. Cheng and L. Mao, Visual detection of melamine in raw milk using gold nanoparticles as colorimetric probe, *Food Chem.*, 2010, **122**(3), 895–900.
5 C. Tian, S. Shin, Y. Cho, Y. Song and S.-Y. Cho, High Spatiotemporal Precision Mapping of Optical Nanosensor Array Using Machine Learning, *ACS Sens.*, 2024, **9**(10), 5489–5499.
6 X. Cao, A. Gao, J.-T. Hou and T. Yi, Fluorescent supramolecular self-assembly gels and their application as sensors: A review, *Coord. Chem. Rev.*, 2021, **434**, 213792.
7 K. Ariga, M. Nishikawa, T. Mori, J. Takeya, L. K. Shrestha and J. P. Hill, Self-assembly as a key player for materials nanoarchitectonics, *Sci. Technol. Adv. Mater.*, 2019, **20**(1), 51–95.
8 B. Roy, P. Bairi and A. K. Nandi, Supramolecular assembly of melamine and its derivatives: nanostructures to functional materials, *RSC Adv.*, 2014, **4**(4), 1708–1734.

9 Y. Geng, H. Dai, S. Chang, F. Hu, Q. Zeng and C. Wang, Formation of C = C Bond via Knoevenagel Reaction between Aromatic Aldehyde and Barbituric Acid at Liquid/HOPG and Vapor/HOPG Interfaces, *ACS Appl. Mater. Interfaces*, 2015, **7**(8), 4659–4666.
10 G. Yin, Y. Ma, Y. Xiong, X. Cao, Y. Li and L. Chen, Enhanced AIE and different stimuli-responses in red fluorescent (1, 3-dimethyl) barbituric acid-functionalized anthracenes, *J. Mater. Chem. C*, 2016, **4**(4), 751–757.
11 D. D. Prabhu, K. Aratsu, M. Yamauchi, X. Lin, B. Adhikari and S. Yagai, Supramolecular polymerization of hydrogen-bonded rosettes with anthracene chromophores: regio-isomeric effect on nanostructures, *Polym. J.*, 2017, **49**(1), 189–195.
12 F. Rasool, G. Wu, I. Shafiq, S. Kousar, S. Abid, N. Alhokbany and K. Chen, Heterocyclic Donor Moiety Effect on Optical Nonlinearity Behavior of Chrysene-Based Chromophores with Push–Pull Configuration via the Quantum Chemical Approach, *ACS Omega*, 2024, **9**(3), 3596–3608.
13 E. Manandhar and K. J. Wallace, Host–guest chemistry of pyrene-based molecular receptors, *Inorg. Chim. Acta*, 2012, **381**, 15–43.
14 B. Carsten, J. M. Szarko, H. J. Son, W. Wang, L. Lu, F. He, B. S. Rolczynski, S. J. Lou, L. X. Chen and L. Yu, Examining the effect of the dipole moment on charge separation in donor–acceptor polymers for organic photovoltaic applications, *J. Am. Chem. Soc.*, 2011, **133**(50), 20468–20475.
15 H. Shen, Y. Li and Y. Li, Self-assembly and tunable optical properties of intramolecular charge transfer molecules, *Aggregate*, 2020, **1**(1), 57–68.
16 M. Z. Ullah, S. A. Shahzad, M. A. Assiri, H. Irshad, S. Rafique, S. A. Shakir and A. Mumtaz, An extensive experimental and DFT studies on highly selective detection of nitrobenzene through deferasirox-based new fluorescent sensor, *Spectrochim. Acta, Part A*, 2024, **306**, 123607.
17 A. P. Demchenko, K.-C. Tang and P.-T. Chou, Excited-state proton coupled charge transfer modulated by molecular structure and media polarization, *Chem. Soc. Rev.*, 2013, **42**(3), 1379–1408.
18 H. V. Barkale and N. Dey, Tuning Sensing Efficacy of Oligo (phenylenevinylene) Based Chromogenic Probes: Effect of Alkyl Substituents on Metal Ion Detection at Micelle-Water Interface, *Chem. – Asian J.*, 2024, e202400058.
19 R. S. Fernandes and N. Dey, Exploring the Synergistic Effect of Aggregation and Hydrogen Bonding: Fluorescent Probe for Dual sensing of Phytic Acid and Uric Acid, *J. Mater. Chem. B*, 2024, 11789–11799.
20 H. V. Barkale and N. Dey, Functionalized cyanostilbene-based nano-AIEgens: multipoint binding interactions for improved sensing of gallic acid in real-life food samples, *J. Mater. Chem. B*, 2024, **12**(35), 8746–8756.
21 X. Cao, L. Meng, Z. Li, Y. Mao, H. Lan, L. Chen, Y. Fan and T. Yi, Large red-shifted fluorescent emission via intermolecular π–π stacking in 4-ethynyl-1, 8-naphthalimide-based supramolecular assemblies, *Langmuir*, 2014, **30**(39), 11753–11760.
22 A. Pal and N. Dey, Oxidized Bisindolyl-Based Amphiphilic Probe for Dual Mode Analysis of Heavy Metal Pollutants in Aqueous Medium, *J. Fluoresc.*, 2024, 1–10.
23 T. N. Das, V. N. Moram, P. Viswanath, T. K. Maji and G. Ghosh, Controlling Supramolecular Self-Assembly and Nanostructures: A Comparative Study in the Solution Phase and at the Air-Water Interface, *ACS Appl. Nano Mater.*, 2024, **7**(16), 19311–19319.
24 M. Torkaman, M. Bahrami and M. Dehghani, Influence of temperature on aggregation and stability of asphaltenes. I. Perikinetic aggregation, *Energy Fuels*, 2017, **31**(10), 11169–11180.
25 S. Saha, S. Paul, R. Debnath, N. Dey and B. Biswas, AIE active fluorescent organic nanoparticles based optical detection of Cu^{2+} ions in pure water: a case of aggregation–disaggregation reversibility, *Anal. Methods*, 2024, **16**(7), 1058–1068.
26 S. Chongdar, S. Bhattacharjee, P. Bhanja and A. Bhaumik, Porous organic–inorganic hybrid materials for catalysis, energy and environmental applications, *Chem. Commun.*, 2022, **58**(21), 3429–3460.
27 H. Hashemian, M. Ghaedi, K. Dashtian, S. Khan, S. Mosleh, S. Hajati and D. Razmjoue, Highly sensitive fluorometric ammonia detection utilizing Solenostemon scutellarioides (L.) extracts in MOF-tragacanth gum hydrogel for meat spoilage monitoring, *Sens. Actuators, B*, 2024, **406**, 135354.
28 S. Mondal and N. Dey, Biogenic Polymer-Based Fluorescent Assemblies: Versatile Platforms for Ultrasensitive ATP Detection and Enzyme Assay, *Langmuir*, 2024, **40**(12), 6163–6171.
29 L. M. Obloy, S. Jockusch and A. N. Tarnovsky, Shortwave infrared polymethine dyes for bioimaging: ultrafast relaxation dynamics and excited-state decay pathways, *Phys. Chem. Chem. Phys.*, 2024, **26**(37), 24261–24278.
30 A. J. Ward and B. E. Partridge, Beyond DAD: Proposing a One-Letter Code for Nucleobase-Mediated Molecular Recognition, *J. Mater. Chem. B*, 2025, **13**(2), 485–495.
31 X. Zhang, Y. Bai, J. Deng, P. Zhuang and H. Wang, Effects of Nonaromatic Through-Bond Conjugation and Through-Space Conjugation on the Photoluminescence of Nontraditional *Luminogens*, *Aggregate*, 2024, **5**(3), e517.
32 M. Zareef, Q. Chen, M. M. Hassan, M. Arslan, M. M. Hashim, W. Ahmad, F. Y. H. Kutsanedzie and A. A. Agyekum, An Overview on the Applications of Typical Non-Linear Algorithms Coupled with NIR Spectroscopy in Food Analysis, *Food Eng. Rev.*, 2020, **12**, 173–190.
33 D. Chicco, M. J. Warrens and G. Jurman, The Coefficient of Determination R-Squared Is More Informative than SMAPE, MAE, MAPE, MSE, and RMSE in Regression Analysis Evaluation, *PeerJ Comput. Sci.*, 2021, **7**, e623.
34 M. Fawad, H. Alabduljabbar, F. Farooq, T. Najeh, Y. Gamil and B. Ahmed, Indirect Prediction of Graphene Nanoplatelets-Reinforced Cementitious Composites Compressive Strength by Using Machine Learning Approaches, *Sci. Rep.*, 2024, **14**(1), 14252.
35 A. Gao, Y. Li, H. Lv, D. Liu, N. Zhao, Q. Ding and X. Cao, Melamine Tunable Effect in a Lenalidomide-Based

Supramolecular Self-Assembly System via Hydrogen Bonding, *New J. Chem.*, 2017, **41**(16), 7924–7931.

36 S. Mondal and N. Dey, Comparative Analysis of Monomeric vs. Dimeric Salen Fluorescent Probes: Transition from a Turn-On to Ratiometric Response Towards Nerve Gas Agents in Organic to Aqueous Media, *Mater. Adv.*, 2025, **6**(3), 977–991.

37 M. G. Fisher, *New Hydrogen Bonding Motifs for Anion and Neutral Guest Complexation*, University of Southampton, PhD thesis, University of Southampton, 2009.

38 V. V. Shilovskikh, A. A. Timralieva, P. V. Nesterov, A. S. Novikov, P. A. Sitnikov, E. A. Konstantinova, A. I. Kokorin and E. V. Skorb, Melamine–Barbiturate Supramolecular Assembly as a pH-Dependent Organic Radical Trap Material, *Chem. Eur. J.*, 2020, **26**(70), 16603–16610.

39 N. Dey and S. Bhattacharya, Hydrogen Bonding-Induced Unique Charge-Transfer Emission from Multichromophoric Polypyridyl Ligands: Ratiometric Probing of Methanol Impurity in Commercial Biofuels, *ACS Sustainable Chem. Eng.*, 2021, **9**(50), 17078–17084.

40 R. S. Fernandes and N. Dey, Synthetic Supramolecular Host for D-(−)-Ribose: Ratiometric Fluorescence Response via Multivalent Lectin-Carbohydrate Interactions, *ChemBioChem*, 2022, **23**(13), e202200044.

41 Y. Liu, L. Wang, L. Zhao, Y. Zhang, Z. T. Li and F. Huang, Multiple hydrogen bonding driven supramolecular architectures and their biomedical applications, *Chem. Soc. Rev.*, 2024, **53**, 1592–1623.

42 K. Gao, *et al.*, Thickness-dependent surface reconstructions in non-van der Waals two-dimensional materials, *Phys. Chem. Chem. Phys.*, 2025, **27**(1), 112–118.

43 M. Ran, *et al.*, Conformation-driven exciton transfer in pyrene-sulfone covalent organic frameworks for bifunctional photocatalysis, *J. Mater. Chem. A*, 2025, **13**(2), 1123–1134.

44 A. Afrin and P. C. A. Swamy, Tailoring emission color shifts in mechanofluorochromic-active AIE systems of carbazole-based D−π–A conjugates: impact of π spacer unit variants, *J. Org. Chem.*, 2024, **89**(11), 7946–7961.

45 S. Pise and N. Dey, Modulation in the charge transfer characteristics of flexible bis-benzimidazole probes: independent sensing mechanisms for Hg^{2+} and F^{-}, *Dalton Trans.*, 2025, **54**(7), 2896–2907.

46 W.-L. Li, F.-Z. Kong, Q. Zhang, W.-W. Liu, H. Kong, X.-P. Liu, M.-I. Khan, A. Wahid, S. Saud and H. Xiao, Simple chip electrophoresis titration of neutralization boundary with EDTA photocatalysis for distance-based sensing of melamine in dairy products, *Anal. Chem.*, 2018, **90**(11), 6710–6717.

47 C. Chu, H. Wang, X. Luo, Y. Fan, L. Nan, C. Du and S. Zhang, Rapid detection and quantification of melamine, urea, sucrose, water, and milk powder adulteration in pasteurized milk using Fourier transform infrared (FTIR) spectroscopy coupled with modern statistical machine learning algorithms, *Heliyon*, 2024, **10**(12), e32720.

48 M. Zhang, X. Cao, H. Li, F. Guan, J. Guo, F. Shen, Y. Luo, C. Sun and L. Zhang, Sensitive fluorescent detection of melamine in raw milk based on the inner filter effect of Au nanoparticles on the fluorescence of CdTe quantum dots, *Food Chem.*, 2012, **135**(3), 1894–1900.

49 X.-M. Xu, Y.-P. Ren, Y. Zhu, Z.-X. Cai, J.-L. Han, B.-F. Huang and Y. Zhu, Direct determination of melamine in dairy products by gas chromatography/mass spectrometry with coupled column separation, *Anal. Chim. Acta*, 2009, **650**(1), 39–43.

50 H. V. Barkale and N. Dey, Membrane-bound bisindolylmaleimide-based chromogenic probes: analysis of cyanogenic glycosides in agricultural crops for possible remediation, *ACS Appl. Bio Mater.*, 2024, **8**(1), 189–198.

51 K. S. Pasupuleti, S. Ghosh, N. Jayababu, C. J. Kang, H. D. Cho, S. G. Kim and M. D. Kim, Boron-doped g-C3N4 quantum dots based highly sensitive surface acoustic wave NO2 sensor with faster gas kinetics under UV light illumination, *Sens. Actuators, B*, 2023, **378**, 133140.

52 J. Xiong, B. Sun, S. Wang, S. Zhang, L. Qin and H. Jiang, Label-free direct detection of melamine using functionalized gold nanoparticles-based dual-fluorescence colorimetric nanoswitch sensing platform, *Talanta*, 2024, **277**, 126335.